ADVANCES IN ATMOSPHERIC SCIENCES, VOL. 39, NOVEMBER 2022, 1956–1968

• **Original Paper** •

Reexamination of the Relationship between Tropical Cyclone Size and Intensity over the Western North Pacific

Kexin CHEN[1,2,3], Guanghua CHEN[*1], and Donglei SHI[1,2]

[1]*Key Laboratory of Cloud-Precipitation Physics and Severe Storms*, *Institute of Atmospheric Physics*, *Chinese Academy of Sciences*, *Beijing* 100029, *China*

[2]*University of Chinese Academy of Sciences*, *Beijing* 100049, *China*

[3]*Shanghai Typhoon Institute*, *China Meteorological Administration*, *Shanghai* 200030, *China*

(Received 13 December 2021; revised 4 March 2022; accepted 11 April 2022)

ABSTRACT

This study reexamines the correlation between the size and intensity of tropical cyclones (TCs) over the western North Pacific from the perspective of individual TCs, rather than the previous large-sample framework mixing up all TC records. Statistics show that the positive size-intensity correlation based on individual TCs is relatively high. However, this correlation is obscured by mixing large samples. The weakened correlation based on all TC records is primarily due to the diversity in the size change relative to the same intensity change among TCs, which can be quantitatively measured by the linear regression coefficient (RC) of size against intensity. To further explore the factors that cause the variability in RCs that weakens the size-intensity correlation when considering all TC records, the TCs from 2001 to 2020 are classified into two groups according to their RC magnitudes, within which the high-RC TCs have a larger size expansion than the low-RC TCs given the same intensity change. Two key mechanisms responsible for the RC differences are proposed. First, the high-RC TCs are generally located at higher latitudes than the low-RC TCs, resulting in higher planetary vorticity and thus higher planetary angular momentum import at low levels. Second, the high-RC TCs are susceptible to stronger environmental vertical wind shear, leading to more prolific outer convection than the low-RC TCs. The positive feedback between outer diabatic heating and boundary layer inflow favors the inward import of absolute angular momentum in the outer region, thereby contributing to a larger size expansion in the high-RC TCs.

Key words: tropical cyclone, size and intensity, composite analysis, absolute angular momentum flux budget

Citation: Chen, K. X., G. H. Chen, and D. L. Shi, 2022: Reexamination of the relationship between tropical cyclone size and intensity over the western North Pacific. *Adv. Atmos. Sci.*, **39**(11), 1956–1968, https://doi.org/10.1007/s00376-022-1450-6.

Article Highlights:

- In most tropical cyclones, size and intensity correlate well, especially during the development stage.
- Changing size-intensity relationships from storm to storm impairs the overall size-intensity correlation based on a mixture of all TC records.
- Genesis latitude and environmental vertical wind shear are two major factors affecting the relationship between the size and intensity of a tropical cyclone.

1. Introduction

Accurate forecasting of the intensity and size of the wind field of a tropical cyclone (TC) is of particular interest to mitigate the suffering of TC disasters. Apart from the intensity, generally measured by the maximum sustained wind (V_{max}), the size of TC is also an important parameter characterizing TC wind structure, which is generally represented by the radius of the outermost closed isobar (ROCI) or the radius of certain wind speeds. Several risk analyses have demonstrated that storm surge, the areal coverage of wind disasters, and rainfall flooding are closely related to TC size (Powell and Reinhold, 2007; Irish et al., 2008; Matyas, 2010). As social exposure to TC-related damage is escalating, an in-depth understanding of TC intensity and size changes are of increasing necessity.

Previous research has explored various factors affecting TC size and intensity. For example, the evolution of both size and intensity is shown to depend on the initial vortex

* Corresponding author: Guanghua CHEN
Email: cgh@mail.iap.ac.cn

structure. A larger initial vortex size is generally more favorable for subsequent expansion but less favorable for intensification (Cocks and Gray, 2002; Lee et al., 2010; Xu and Wang, 2010a; Rogers et al., 2013; Carrasco et al., 2014; Chan and Chan, 2014; Martinez et al., 2020). Besides, TCs at lower latitudes are found to intensify rapidly but expand slowly in size (DeMaria and Pickle, 1988; Smith et al., 2011, 2015; Li et al., 2012; Chan and Chan, 2014). Numerous numerical studies showed that increased environmental moisture promotes outer rainbands and thus size expansion in the outer regions (Hill and Lackmann, 2009; Martinez et al., 2020), while reinforced outer convection could also suppress mass and moisture advection toward the inner core region, thus prohibiting intensification (Powell, 1990; Wang, 2009; Xu and Wang, 2010b; Sun et al., 2014; Chen et al., 2018). Strong vertical wind shear (VWS) is detrimental to TC intensification (Merrill, 1984; Elsberry and Jeffries, 1996; Demaria and Kaplan, 1999; Knaff et al., 2004; Tang and Emanuel, 2010). However, size expansion under strong VWS has been pronounced in observational and numerical studies (Kimball and Evans, 2002; Tao and Zhang, 2019). In addition, the intensification rate was also found to be proportional to sea surface temperature (SST; Xu and Wang, 2018a), while the relative SST (TC environmental SST relative to the tropical mean SST) is stated to account for the change in TC size (Lin et al., 2015).

Tropical cyclone (TC) intensification and expansion can be physically interpreted by the convergence of absolute angular momentum (AAM). Holland (1983) detailed the dynamical role and relative contribution of various AAM terms in maintaining TC structure. Furthermore, by conducting numerical experiments, Smith et al. (2009) identified two mechanisms for the spin-up of cyclonic circulation. They suggested that the size expansion is related to the convergence of AAM above the boundary layer to spin up the outer circulation, while the intensification is attributed to the convergence of AAM within the boundary layer to spin up the inner circulation. Based on Quick Scatterometer data, Chan and Chan (2013) also demonstrated that the change in intensity is related to the export of upper-tropospheric AAM, while the change in size is connected with the import of lower-tropospheric AAM.

Previous studies have documented the weak size–intensity correlation for all TC records (e.g., Merrill, 1984; Weatherford and Gray, 1988; Chan and Chan, 2012; Chavas and Emanuel, 2010; Guo and Tan, 2017). For example, using a large sample of TC records over the North Pacific and North Atlantic, Merrill (1984) found that the correlation coefficient between the minimum sea surface pressure and ROCI was only 0.28. Similarly, Guo and Tan (2017) also found a weak correlation of 0.29 between V_{max} and the radius of the 34 kt (1 kt = 0.5144 m s $^{-1}$) wind speed (R34). This weak correlation is suggested to be partly due to the nonlinear size-intensity evolution (Musgrave et al., 2012; Knaff et al., 2014; Wu et al., 2015; Chavas et al., 2016; Song et al., 2020). Specifically, during early intensification, TC size expands along with increasing intensity. After a TC reaches a certain intensity, however, the size can level off (Knaff et al., 2014; Chavas et al., 2016) or even decrease (Wu et al., 2015) with continuous intensification or still expand while the intensity remains quasi-steady (Wang and Toumi, 2018). However, it should be pointed out that the approach, based on a large-sample framework in previous studies, mixes up all TC records and thus fails to capture the unique size-intensity relationship for individual TCs, which can give rise to an overall weak size-intensity correlation.

Physically, both intensity and size are important metrics that explicitly describe the TC wind field. Previous observation and simulation studies examined the lifetime evolution of individual TC size or intensity, revealing a systematic increase in size with intensity during early intensification (Smith et al., 2011; Musgrave et al., 2012; Knaff et al., 2014; Wu et al., 2015; Song et al., 2020). However, how to quantify the size-intensity relationship for individual TCs and explicate the variation of the relationship from storm to storm are not adequately addressed. An in-depth understanding of the size-intensity relationship for individual TCs could help shed light on the large diversity of TC characteristics, such as the presence of a "Weak giant" (large but weak) and "Strong dwarf" (small but strong) TCs, as suggested by Musgrave et al. (2012).

The concerns mentioned above motivate us to investigate the size-intensity relationship during the development stage from the perspective of an individual TC and the potential factors affecting the relationship. The remainder of this paper is organized as follows. Section 2 describes the data used in this study. Section 3 details how various size-intensity relationships among individual TCs influence the overall size-intensity correlation. Potential factors affecting the size-intensity relationships and the related physical explanations are presented in section 4. the summary and discussion are given in section 5.

2. Data and methodology

The 6-hourly TC location and intensity (V_{max}) information from 2001 to 2020 over the Western North Pacific (WNP) are obtained from the Joint Typhoon Warning Center (JTWC) best track data, which also provides the quadrant wind radius estimations of gale-force wind (34 kt), damaging-force wind (50 kt), and hurricane-force wind (65 kt) from 2001 onward. The quadrant-averaged R34 is adopted as the size metric in this study, given that it is operationally important for issuing warnings of wind destructiveness (Knaff et al., 2007; Bender et al., 2017). Because the estimations of R34 from JTWC are relatively subjective without post-season revision (Knaff, 2006; Knaff et al., 2007; Song and Klotzbach, 2016), the information on TC size and intensity archived by the Japan Meteorological Agency (JMA), which includes V_{max} and the longest and shortest radii of 30 kt wind, is also obtained to further support our analyses. In contrast to JTWC, the wind radii estimations have been

updated by the post-analysis before the final documentation in JMA (Knaff, 2006; Song and Klotzbach, 2016). Consistent with previous studies (Song and Klotzbach, 2016; Song et al., 2020), the JMA TC size is defined as the average of the longest and shortest 30 kt wind radii (R30).

The atmospheric factors, including wind, relative humidity, and SST, are obtained from the European Center for Medium-Range Weather Forecasts (ECMWF) fifth generation global atmospheric reanalysis (ERA5), with a horizontal resolution of 0.25° (Hersbach et al., 2020). In addition, precipitation estimations from the Global Precipitation Measurement (GPM) mission satellites are used as a proxy for TC convection. The GPM precipitation products are produced by the integrated multi-satellite retrieval algorithm, and its final run version used in this study has a temporal and spatial resolution of 30 min and 0.1°, available from 2000 to the present.

As pointed out by Song et al. (2020), the time corresponding to a TC first reaching its lifetime maximum intensity (T_{LMI}) seldom coincides with that of its lifetime maximum size (T_{LMS}). The development stage in this study is specified as the period from the time when TC first intensifies into a tropical storm (TS) and the earlier of T_{LMI} and T_{LMS}. Here, the earlier of T_{LMI} and T_{LMS} is designated as the ending time of the development stage to ensure that both the intensity and size are developing during this stage. Furthermore, strict data screening was carried out as follows: (1) TC records north to 35°N are removed to eliminate the possible effect of extratropical transition; (2) TC records with R34/R30 greater than the distance from the TC center to the nearest land are excluded to eliminate the influence of terrain; (3) TCs with at least 15 valid size records during the development stage are retained to ensure sufficient samples for individual TCs. Based on the criteria above, 2572 records are selected from the lifetime of 73 TCs from the JTWC and 2080 records from the lifetime of 58 TCs from the JMA, containing 1389 and 1103 records from the development stage of each TC, respectively. Note that the smaller sample size of JMA is mainly due to the lack of records from 2020.

3. Size-intensity relationship for individual TCs

We start by giving an overall picture of how different calculation methods affect the correlation between the size and intensity of the TC. The first method, adopted by previous studies (e.g., Merrill, 1984; Guo and Tan, 2017), treats the records from all TCs as a whole, referred to as "all". The second method used in this study is based on the perspective of individual TCs. The size-intensity correlation coefficients are first calculated for individual TCs and then averaged for all TCs, referred to as "each". Note that despite the relatively small sample size of each TC, due to coarse temporal resolution in the best track dataset, most TCs selected from JTWC and JMA have significant size-intensity correlations [the correlation coefficient between size and intensity is referred to as R hereinafter to be included in the electronic supplementary material (ESM)]. Specifically, throughout the lifetime, the R of only 3 out of 73 JTWC TCs and 5 out of 58 JMA TCs do not reach the 95% confidence level based on the Students' t-test. When focusing on the development stage, the R of only 3 (JTWC) and 2 (JMA) TCs fail to satisfy a 95% confidence level.

The R distributions calculated for individual TCs during the development stage and throughout their lifetime are shown in Fig. 1. As shown in Fig. 1a, approximately 75% of the JTWC TCs have a size-intensity correlation greater than 0.50 in the context of the entire lifetime, with an average R of 0.67 ("Lif, each"). The R decreases to 0.53 if all JTWC records are mixed ("Lif, all"). When focusing on the development stage, the size-intensity correlation is enhanced and much greater than that of the total samples (0.83 versus 0.61). The results remain qualitatively consistent when using the JMA dataset (Fig. 1b), that is, the size-intensity correlation of individual TCs is stronger compared to that from the mixture of all TCs records for the entire lifetime (0.67 versus 0.44), especially during the development stage (0.84 versus 0.40).

It should be pointed out that the size-intensity correlations in JTWC and JMA are higher than in previous studies, which is primarily due to the subjective and intensity-dependent method used in estimating the wind radii in these agencies (Knaff, 2006; Song and Klotzbach, 2016). For example, the Huntley model, used in JTWC as a reference for the operational forecaster, is an empirical parametric model incorporating intensity and the radius of maximum wind (Cocks and Gray, 2002; Knaff, 2006). However, the objective of this study is to examine how the different calculation methods affect the size-intensity correlation. As shown above, there is a significant decrease in R from the perspective of individual TCs to all TC records, which suggests that the size-intensity correlation can be potentially affected by the calculation method. This result is further supported by the JMA dataset, in which the wind radius estimations are more objective since being updated by the post-analysis, thereby reducing the dependence of size estimation on intensity (Knaff, 2006; Song and Klotzbach, 2016).

Nevertheless, the qualitative consistency in both the JTWC and JMA datasets confirms an intrinsic correlation between size and intensity for individual TCs, which is obscured by mixing all TC records. In addition, the inherent correlation is more robust during the development stage, given the narrower spread of the boxplot. Since the development stage presents a more robust correlation, attention will be paid exclusively to this period in the rest of this study.

To clarify why the size-intensity correlation of all samples is lower than that of the individual TCs, Fig. 2a shows the V_{max}-R34 diagram during the development stage of all selected TCs. Records during the development stage for the 73 TCs exhibit a size-intensity correlation of 0.61. Although the size and intensity increase synchronously in most TCs, the expansion in size relative to intensification varies signifi-

cantly. To illustrate this fact, two representative TCs are chosen, one with a relatively high expansion rate [Haima (2016)] and one with a low expansion rate [Chaba (2016)]. The evolution of their size and intensity relationship is clearly marked in Fig. 2a by red and blue lines, respectively. During their development stage, the two TCs have similar intensity changes of about 110 kt, whereas the change in the R34 of Haima is much greater than that of Chaba (200 km versus 80 km). The correlation coefficient between V_{max} and R34 of Haima and Chaba both reach 0.88 or even higher. When combining all records of two TCs, the correlation reduces to 0.61. The decreased correlation suggests that mixing records of TCs with distinct changes in size relative to the same intensity change not only impairs the overall size-intensity correlation but also obscures the strong correlation inherent to each TC.

To quantify the size change relative to the same intensity change for individual TCs, linear regression is applied to each TC. The linear regression coefficient of R34 against V_{max} (hereafter referred to as RC) can be considered a mea-

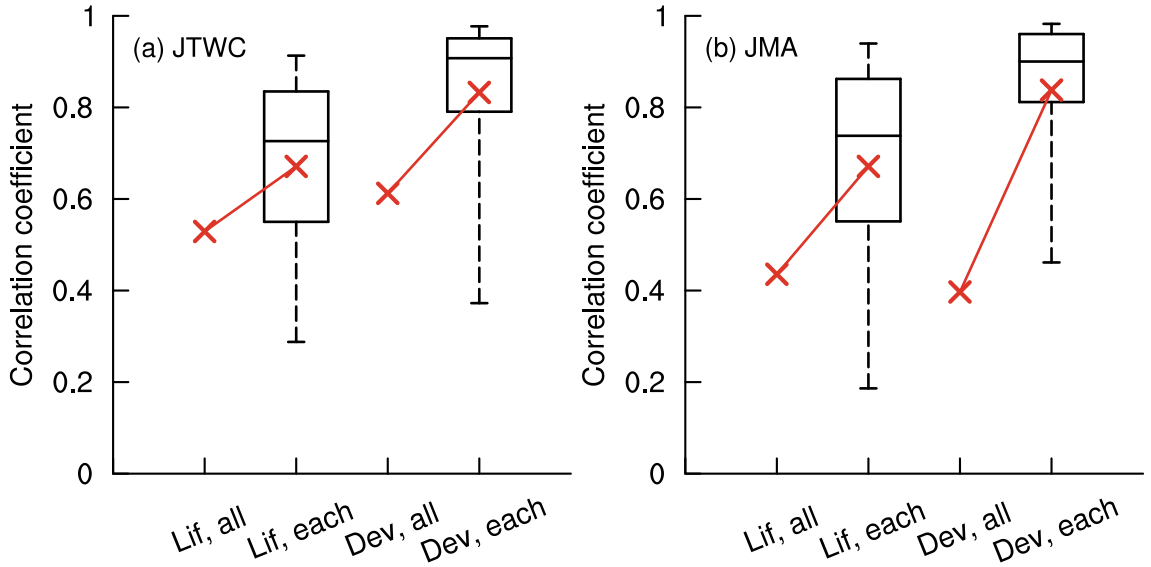

Fig. 1. Comparison of the correlation coefficients between size and intensity using different calculation methods based on (a) JTWC and (b) JMA datasets for different lifetime stages. On the abscissa, "Lif" and "Dev" represent the entire lifetime and development stage, while "all" and "each" represent different calculation methods, respectively. The red × in the "all" group represents the correlation coefficient for all of the TCs' records, which exceeds the 99% confidence level of the Student's *t*-test. While in the "each" group, the size-intensity correlation of each TC is calculated, the 25th, 50th, and 75th percentiles of the correlation coefficient of individual TCs are given by the box, and the whiskers extend to the 5th and 95th percentiles. The red × in the "each" group represents the average correlation coefficient for all individual TCs.

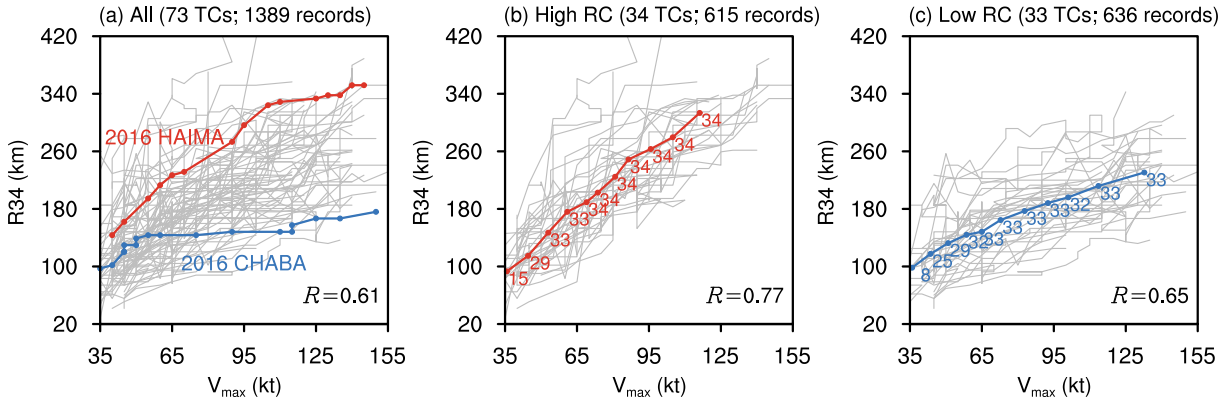

Fig. 2. (a) V_{max}-R34 diagram of all TCs based on the JTWC dataset; representative TCs with high and low RCs are marked by red and blue lines, respectively. Panels (b) and (c) show V_{max}-R34 diagrams for high-RC and low-RC TCs, with the composite evolutions of V_{max}-R34 colored red and blue with ten dots. Note that the time series of V_{max}-R34 are first normalized by the duration of the development stage for each TC before the composition. The number below each dot denotes the number of TCs with valid records. The correlation coefficient between V_{max} and R34 for all the records of selected TCs is displayed in the bottom right corner of each panel.

surement of the size-intensity relationship. Namely, a large RC stands for a greater expansion in size relative to intensification. The converse is true for a small RC. To facilitate a comparison among the TCs with various RCs, the TCs are classified into two groups according to the 50th percentile of the RC. TCs within the top 50% RCs are referred to as high-RC TCs (34), and the remaining TCs are classified as low-RC TCs (33). Note that out of a total of 73 TCs; there are 6 TCs whose V_{max} and R34 during the development stage are not positively correlated at the 99% confidence level based on the Students' *t*-test, accounting for 8% of the total samples. These TCs are excluded prior to classification, allowing for a focus on TCs with a significant size-intensity correlation.

Figures 2b and 2c show the V_{max}-R34 diagrams for the high-RC and low-RC TCs, respectively, manifesting a distinct evolution tendency of size and intensity between these two groups. Because the duration of the development stage varies among TCs, the time series of the V_{max}-R34 diagram of each TC is first normalized by its development period (T_{dev}) for the convenience of the composite. Then, for each TC, V_{max} and R34 are linearly interpolated from 0 to 1 T_{dev} with an interval of 0.1 T_{dev}. Finally, the interpolated data from different TCs are composited at each normalized time point. Composite V_{max}-R34 profiles for high-RC and low-RC TCs are depicted as the red and blue lines in Figs. 2b and 2c, respectively. Note that some TCs in JTWC have missing R34 records before 0.4 T_{dev}. The steeper slope of the composited V_{max}-R34 regression line in the high-RC group suggests an evident larger expansion in size relative to the same intensity change compared to the low-RC group (Figs. 2b, c). Similar to the discussion above, the size-intensity correlations of all records in both groups are stronger than the counterpart of the total TCs, evidenced by an R of 0.77 for the high-RC TCs and 0.65 for the low-RC TCs.

As displayed in Figs. 3a and 3b, further statistical analysis shows that the high-RC TCs possess an average expansion rate of 47.6 km d^{-1} according to the R34 from the JTWC, which is in significant contrast to that of the low-RC TCs of 36.6 km d^{-1}. For comparison, there is no significant difference in the intensification rate between the high-RC and low-RC TCs, suggesting that the steeper slope of the composited V_{max}-R34 profile of the high-RC TCs is primarily caused by the faster expansion of R34. Furthermore, the comparison is also made in terms of size and intensity distribution at the end of the development stage (Figs. 3c, d). Most high-RC TCs (94%) have an ultimate size larger than 250 km with a peak in the 300–500 km range, whereas low-RC TCs have the largest portion in the 200–250 km range. The differences in size distribution between these two groups are significant at the 99% level based on a two-tailed Mann-Whitney U test. On the other hand, although the intensification rates of the two groups differ marginally, the low-RC TCs generally skew more toward higher intensity than the high-RC TCs at the end of the development stage, which is mainly due to the longer development duration in the low-RC TCs (5.3 vs. 4.6 days).

The above results demonstrate that the relatively weak size-intensity correlation in a large-sample framework revealed in previous literature can be largely attributed to the variation in size expansion among TCs. The following section will investigate the potential factors and related mechanisms responsible for the difference in size expansion between the high-RC and low-RC groups.

4. Potential mechanisms leading to the variability of size expansion

4.1. *AAM flux budget*

As suggested by previous studies (Holland, 1983; Smith et al., 2009; Chan and Chan, 2013), the size expansion is related to the low-level convergence of AAM at large radii, which spins up the tangential winds at the outer region. The AAM per unit mass is composed of two parts,

$$\mathrm{AAM} = v_\theta r + \frac{1}{2} f r^2 , \tag{1}$$

where v_θ is the tangential wind, r is the radius relative to the TC center, and f is the Coriolis parameter. The terms on the right-hand side of Eq. (1) are the relative angular momentum (RAM) and earth angular momentum (EAM), respectively. To further unravel the difference in size expansion between the high-RC and low-RC TCs, the AAM flux (AAMF) analysis is conducted, as in Chan and Chan (2013). The AAMF across the radius r relative to the TC center is given by:

$$\mathrm{AAMF}(r) = r\overline{v_\theta}\,\overline{v_r} + r\overline{v'_\theta v'_r} + \frac{f_0 r^2 \overline{v_r}}{2} + \frac{r^2 \overline{f v'_r}}{2} , \tag{2}$$

where v_r and f_0 are the radial wind and Coriolis parameter at the TC center. The overbar and prime denote the azimuthal average and deviation from the azimuthal average, respectively. The four terms on the right-hand side of Eq. (2) are the axisymmetric RAM flux, the asymmetric RAM flux, the axisymmetric Coriolis torque, and the asymmetric component, abbreviated as SRAMF, ARAMF, SCT, and ACT.

As suggested by previous studies (Tsuji et al., 2016), the changes in R34 are closely related to momentum transport relative to R34. However, R34 changes with time and case during the development stage. Therefore, the radius is normalized by R34 for the convenience of the composite and comparison. Figure 4 shows the radius-height cross-section of the terms contributing to the AAMF averaged during the development stage, with the radius normalized by R34 each time. Because the magnitudes of the asymmetric terms are relatively small, only the SRAMF and SCT are shown. Note that only the results outside of R34 are shown since they are directly related to the changes of R34. It is evident that there is a greater negative AAMF at low-to-mid levels in the high-RC TCs compared to the low-RC TCs (Figs. 4a, b), with the largest difference appearing below 800 hPa (Fig. 4c). This

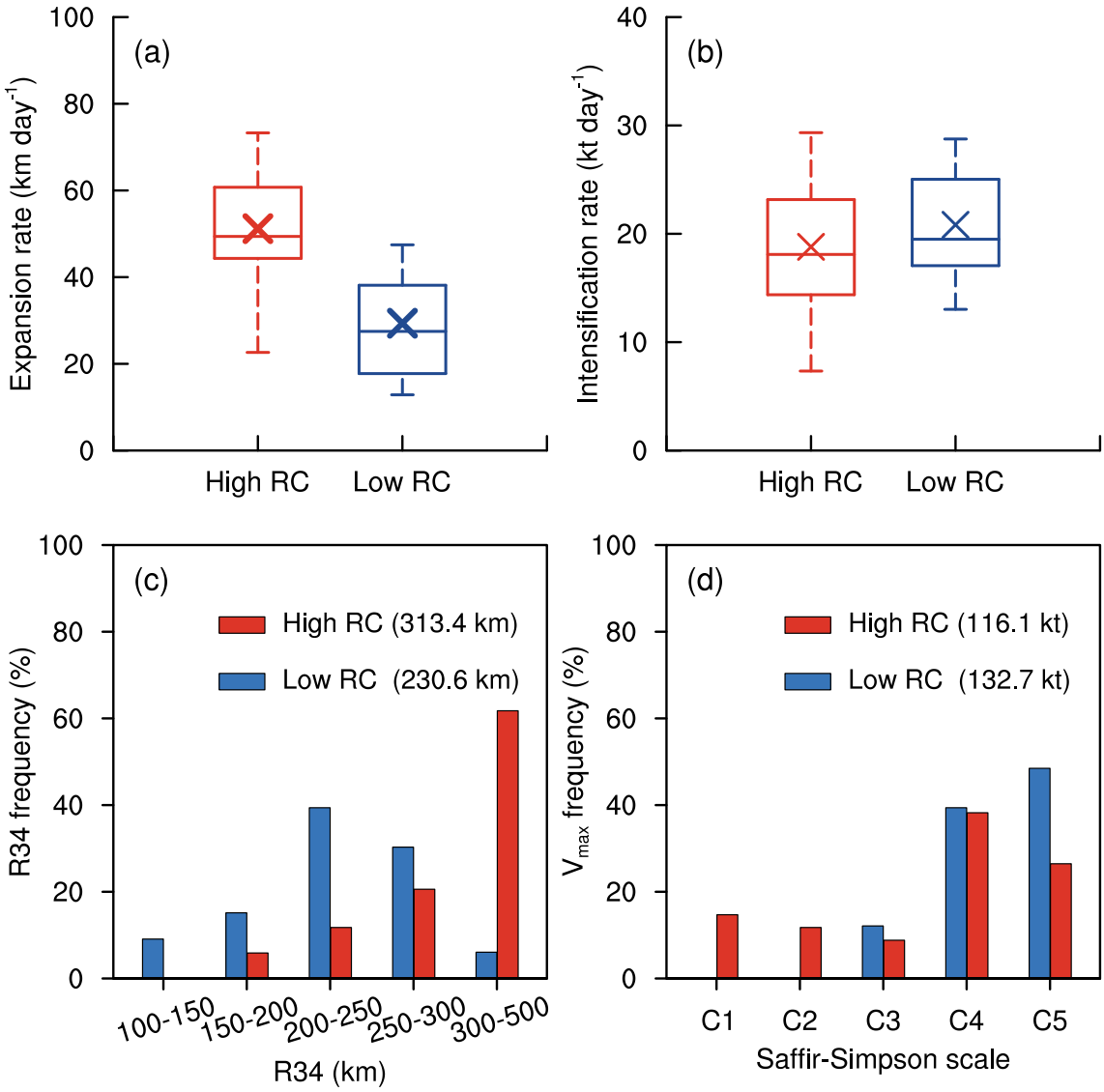

Fig. 3. Box-and-whisker plots of the (a) expansion rate and (b) intensification rate for the (red) high-RC and (blue) low-RC TCs. In each box, the 25th, 50th, and 75th percentiles are indicated; the whiskers extend from 5th to 95th percentiles. The × represents the mean. The bolded × indicates that the mean difference between the two groups exceeds the confidence level at 99% based on a two-tailed Mann-Whitney U test. Percentage distribution of (c) R34 and (d) V_{max} are given at the end of the development stage for the high-RC (red bar) and low-RC (blue bar) TCs. The average values are given in parentheses. C1 to C5 on the abscissa of (d) refer to the five intensity categories based on the Saffir-Simpson scale.

indicates a greater import of AAM in the boundary layer in the high-RC TCs, consistent with the higher expansion rate of R34. The two contributing terms, SRAMF and SCT, are stronger in the high-RC TCs than their lower counterparts. Furthermore, the difference in SCT is larger than that in SRAMF, especially in the region outside of 1.4 times R34, suggesting that SCT plays a primary role in the difference of AAMF and, therefore, in the different expansion rates between these two groups of TCs. Holland (1983) also emphasized that the SCT term is essential to maintain the cyclonic acceleration at the lower inflow layer.

To gain further insight into the differences in AAMF and size expansion, Fig. 5 displays the temporal evolutions of R34, SRAM, and SCT. The time is normalized by the duration of the development stage of each TC for the convenience of composite. The SRAM and SCT are averaged between 1 and 3 times R34 and from the surface to 800 hPa during the development stage. As expected, the normalized time series of R34 has a close correlation with the importation of AAM contributed by the SRAMF and SCT terms (Figs. 5a, b). The SRAMF and SCT are higher in the high-RC TCs than in the low-RC TCs, and thus their combined effect positively contributes to a larger size expansion in the former. Meanwhile, the difference between SCT and SRAMF is enlarged in the latter half of the development stage with a stronger SCT amplification than SRAMF (Fig. 5c).

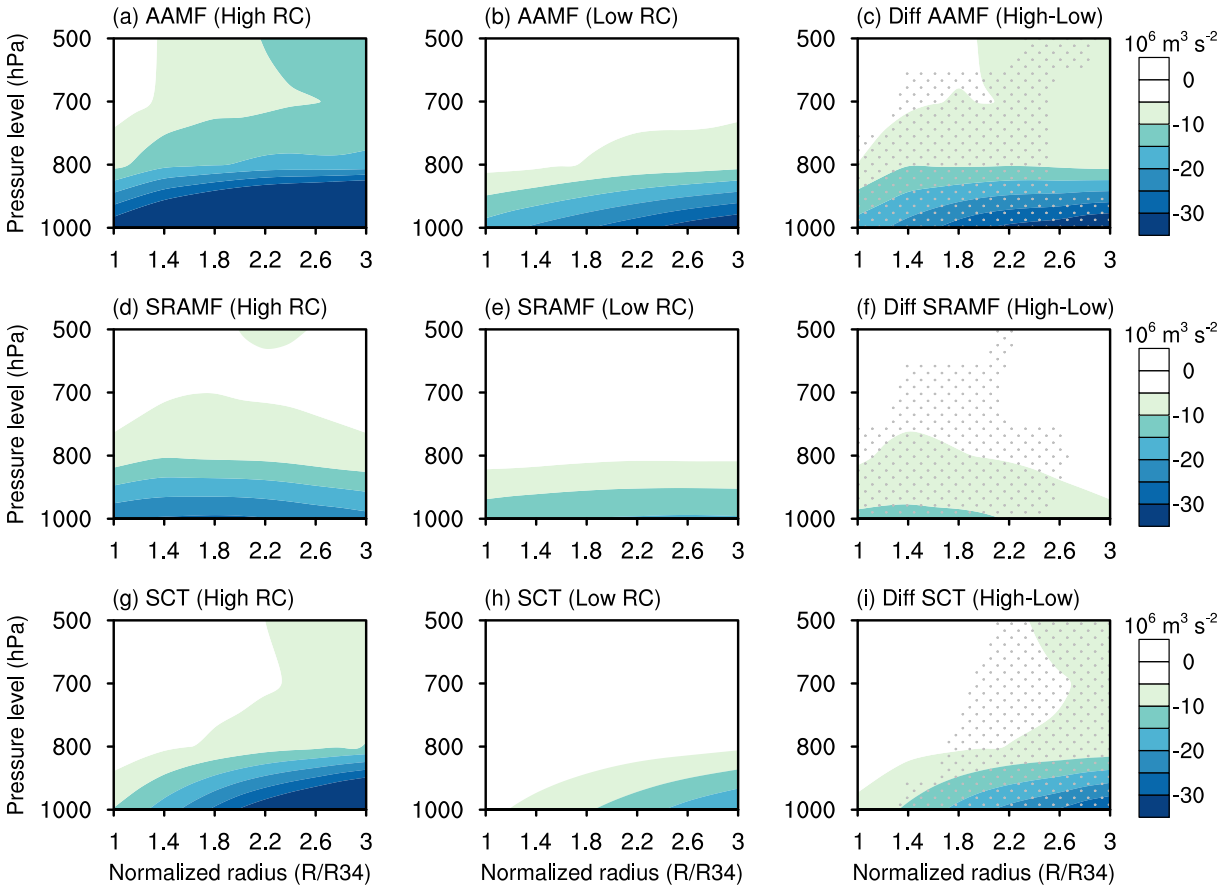

Fig. 4. Composited radius-height cross-sections of (a, b) total AAMF, (d, e) SRAMF, and (g, h) SCT for the (a, d, g) high-RC and (b, e, h) low-RC TCs averaged during the development stage, and the difference in (c) total AAMF, (g) SRAMF and (f) SCT between the high-RC and low-RC TCs. The abscissa represents the radius normalized by R34 at each time during the development stage. Differences between the high-RC and low-RC TCs exceed the 99% confidence level based on a 1000-sample bootstrap test and are marked by the grey dots in (c, f, i).

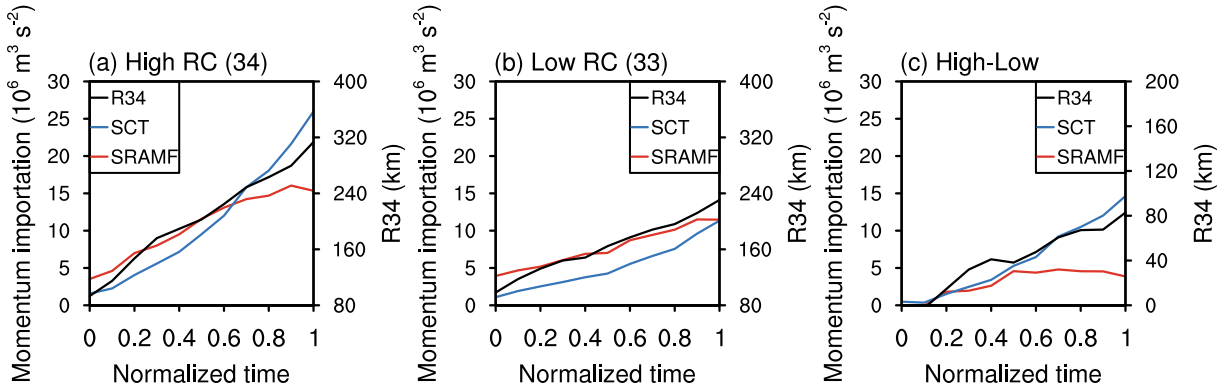

Fig. 5. Time series of the composite SRAMF (red line) and SCT (blue line) averaged between 1–3 times *R*/R34 and between 1000–800 hPa, and R34 (black line) for the (a) high-RC and (b) low-RC TCs and (c) differences between them. Time is normalized by the duration of the development stage of individual TCs.

4.2. *Possible mechanisms for the AAMF difference*

Since the SCT term dominates the difference in AAMF between the high-RC and low-RC TCs during the development stage, the two parameters f and v_r in SCT are further investigated. The genesis locations and tracks of the two groups of TCs are displayed in Fig. 6. The high-RC TCs are frequently distributed in the western portion of WNP and to the north of 15°N (Fig. 6a), while the low-RC TCs tend to form in the eastern portion and to the south of 15°N (Fig. 6b). The difference in track density reveals a clear northeast-southwest dipole pattern (Fig. 6c). The high-RC TCs feature higher track density in the region of 130°–150°E, 15°–25°N,

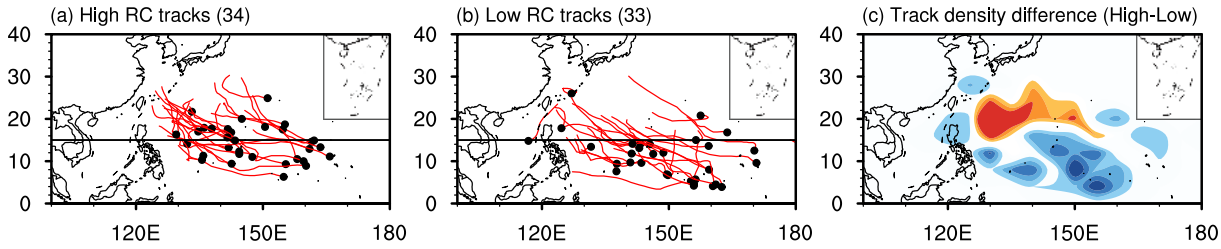

Fig. 6. Genesis locations (black dots) and tracks during the development stage (red lines) for the (a) high-RC and (b) low-RC TCs, where the black line indicates the location of 15°N. Panel (c) displays the differences in track density between the high-RC and low-RC TCs, obtained by counting the TC tracks in each 4° latitude × 5° longitude box. Shaded areas are contoured from –16 to 16 at intervals of 4 with positive (negative) values shaded in red (blue).

while the low-RC TCs over 140°–160°E, 0°–15°N. Further statistical analysis reveals that the genesis latitude of high-RC TCs is significantly higher than that of low-RC TCs, with a difference of 3.1° latitude, and this difference satisfies a 99% confidence level based on the Mann-Whitney U test. Owing to the more poleward occurrence, the high-RC TCs generally evolve in an environment with higher planetary vorticity (f), which favors a larger SCT in the outer region, in good agreement with Chan and Chan (2014), who demonstrated that the Coriolis torque due to the import of earth's angular momentum contributes to a faster size expansion in the TCs at higher latitudes than in those at lower latitudes.

In addition to the Coriolis parameter (f), the SCT also depends on the strength of low-level inflow v_r. Figure 7 depicts the evolution of the low-level inflow averaged between 1 and 3 times R34 in the two groups. Clearly, the high-RC TCs have stronger low-level inflows over most of the development stage (after the normalized time of 0.2). As a result, the joint contribution of the stronger low-level inflow and the higher planetary vorticity leads to a much higher SCT in the high-RC TCs. In addition, the larger low-level inflow can also contribute to increasing the SRAMF in the high-RC TCs, as shown in Figs. 4d and 4f.

To further investigate what causes the difference in v_r, the initial R34 and several environmental factors potentially influencing the strength of the low-level inflow, as stated in the introduction, are compared. The thermodynamic factors include SST, defined here by the average in a 2°–5° latitude annulus relative to the TC center, and the environmental relative humidity, represented by the 500–700 hPa mean within an annulus of 2°–8° latitude. The dynamic factor is the environmental VWS, defined as the TC-removal wind difference between 200 and 850 hPa averaged within an annulus of 5°–10° latitude. Here, the wind fields related to TCs are removed using the filtering algorithm proposed by Kurihara et al. (1993).

Although previous studies (Xu and Wang, 2010b; Chan and Chan, 2014; Martinez et al., 2020) demonstrated that the initial size can modulate the boundary layer inflow and thus the AAM convergence in the outer region, the initial sizes (defined as R34 when TC first reaches TS intensity in this study) are pretty similar in these two groups (not shown). In addition, different from previous studies, in which higher SST and environmental humidity are potential

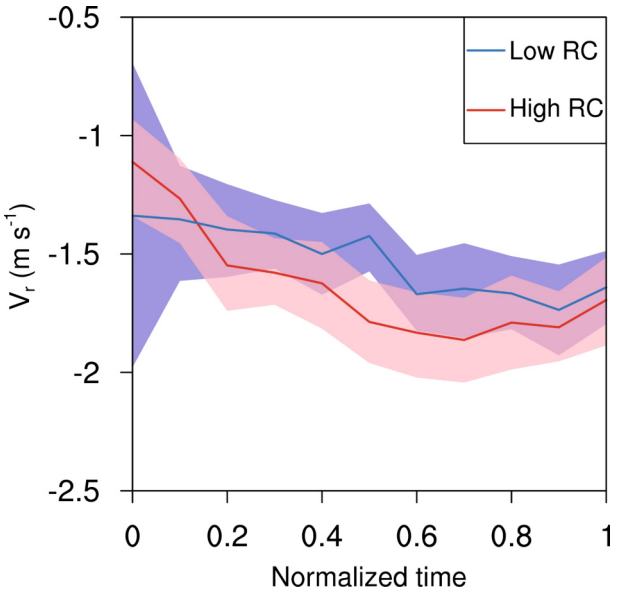

Fig. 7. Composited time series of the radial flow averaged between 1–3 times R/R34 and between 1000 and 800 hPa for the (red line) high-RC and (blue line) low-RC TCs within a 95% confidence interval calculated from a 1000-sample bootstrap approach (shading). Time is normalized by the duration of the development stage of individual TCs.

factors that promote the expansion of TC size (Hill and Lackmann, 2009; Xu and Wang, 2018b; Martinez et al., 2020), the differences in SST and RH between high-RC and low-RC TCs are insignificant, as shown in Figs. 8a and 8b, implying that these two parameters may exert only minor influences on the difference in the expansion rate during the development stage.

Unlike the insignificant distinction in the thermodynamic parameters, the difference in VWS is notable, with stronger environmental wind shear in the high-RC TCs than in low-RC TCs during the development stage (Fig. 9c). To elucidate upon this VWS difference, the upper- and low-level wind fields surrounding the TCs are examined. The composites of TC-removed winds for the high-RC and low-RC TCs at 200 and 850 hPa are shown in Fig. 9. The large-scale anticyclones at 200 hPa are similar in pattern and strength for the high-RC and low-RC TCs (Figs. 9a, b). In contrast, although both 850-hPa wind fields take on a monsoon gyre pattern,

the southwesterly and southeasterly flows on the southern and northern sides of the monsoon gyre are much more vigorous in the high-RC TCs (Figs. 9c, d), which is a key source resulting in a higher VWS. Lee et al. (2010) also pointed out the existence of strong low-level southwesterly flows in the outer region south of large TCs throughout the development stage.

As reported in previous studies (Tsuji et al., 2016; Martinez et al., 2020), the TC size expansion is attributed to the low-level inward transport of momentum related to the sec-

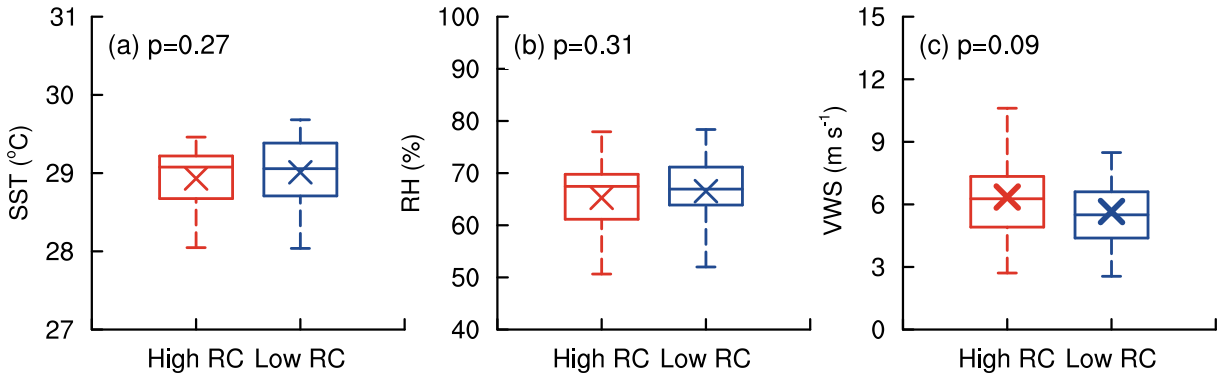

Fig. 8. As in Fig. 6, but for the sea surface temperature (°C), mid-level relative humidity, and the magnitude of vertical wind shear. The bolded × indicates that the mean difference between the two groups is significant at the 90% confidence level.

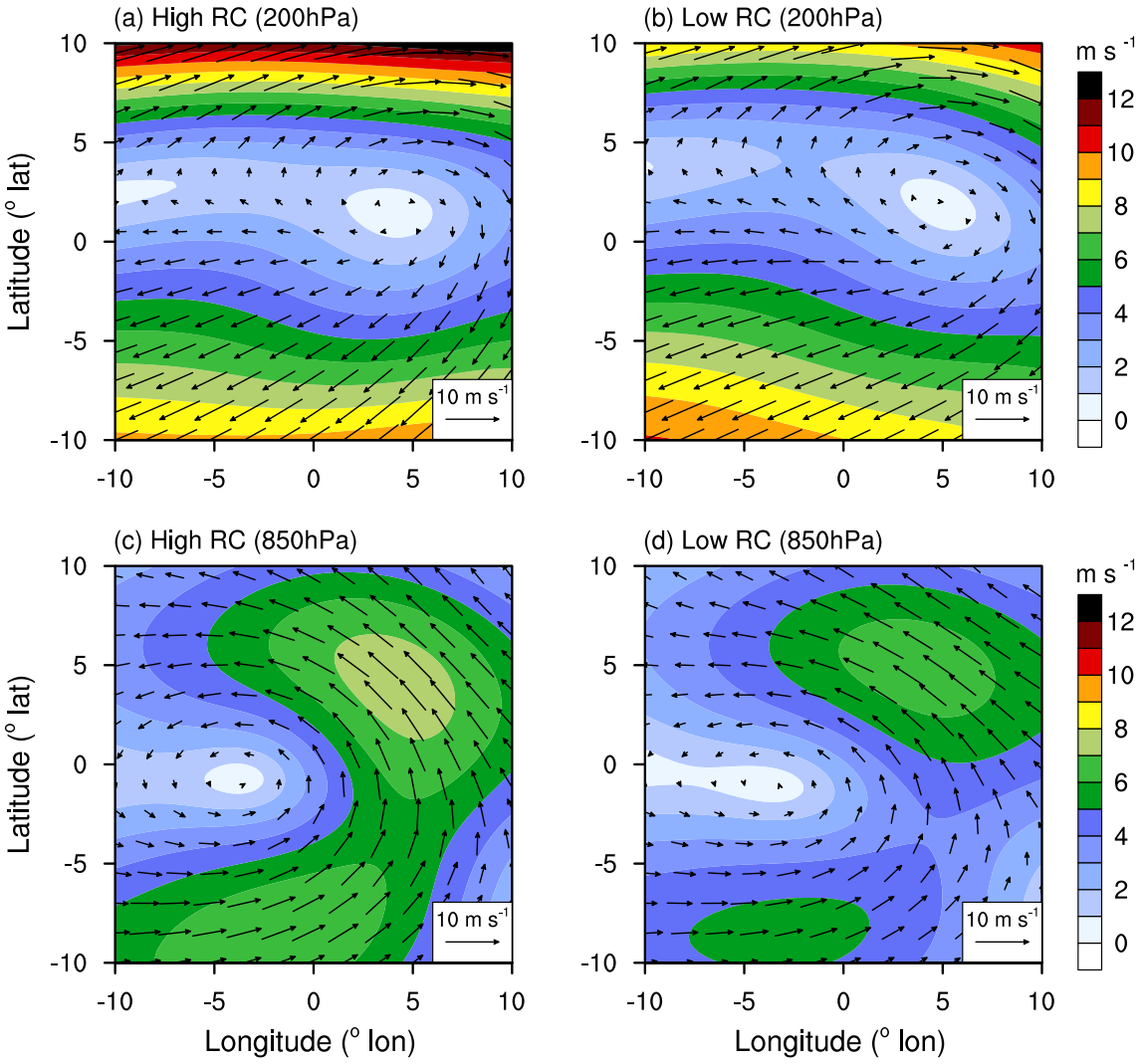

Fig. 9. Composites of wind speed at 200 and 850 hPa (shaded, m s^{-1}) and wind vector (arrow) relative to the center of (a, c) high-RC and (b, d) low-RC TCs.

ondary circulation, driven by the diabatic heating through precipitation condensation. Further, the TC precipitation distribution can be largely affected by environmental VWS. Specifically, VWS can promote the development of outer precipitation in the downshear and downshear-left quadrants (Li et al., 2017; Chan and Chan, 2018; Kim et al., 2018, 2019; Tao and Zhang, 2019); thus, broadening the wind field in these quadrants. Therefore, the influence of VWS on the TC wind field is exerted through the low-level inflow driven by diabatic heating released in precipitation (Hill and Lackmann, 2009; Wang, 2009; Martinez et al., 2020).

To illustrate the modulation of VWS on the evolution of TC rainfall, Fig. 10 presents the composites of precipitation, which are rotated relative to the VWS direction, in the high-RC and low-RC TCs at the beginning (T0), middle (T50), and the end (TE) of the development stage, respectively. Both the high-RC and low-RC TCs exhibit a less-concentrated rainfall distribution at T0 (Figs. 10a, d), while the stronger VWS promotes precipitation in the downshear quadrant resulting in a more asymmetric distribution in the high-RC TCs. A pronounced difference occurs at T50, where the strong rainfall, greater than 12 mm h^{-1}, gradually shifts to the outer region in the high-RC TCs (Fig. 10b). In contrast, the strong precipitation in the low-RC TCs tends to be organized towards small radii (Fig. 10e). In high-RC TCs, the precipitation expands radially outward with time, and eventually, a wider precipitation band with a maximum located in the downshear-left quadrant forms at the end of the development stage (Fig. 10c). In contrast, the vigorous rainfall in the low-RC TCs is confined to a small radius, leading to a stronger and more compact precipitation structure in the inner core region (Fig. 10f).

Figure 11 further shows the radial profiles of azimuthally-averaged precipitation for these two groups of TCs. At small radii (<1° latitude), the precipitation rate of low-RC TCs is significantly higher than that of high-RC counterparts, while the situation is reversed in the outer region (>1° latitude), suggesting that the presence of stronger shear generally amplifies precipitation in the outer region, but hinders precipitation around the TC center (Kimball and Evans, 2002; Tao and Zhang, 2019). The stronger outer precipitation accounts for the stronger convectively induced low-level inflow in the outer region, indicating that a larger VWS may play an important role in the faster size expansion in the high-RC TCs.

In summary, the above statistical analyses suggest two major mechanisms responsible for the faster size expansion of high-RC TCs during the development stage. The first is higher latitude, which enhances the incorporation of environmental earth rotation and, thus, the low-level cyclonic acceleration at larger radii through the SCT terms. The second is a stronger environmental VWS that promotes outer precipitation to enhance convectively induced low-level inflow in the outer region. Finally, these two effects cooperatively contribute to a large inward import of both the planetary and relative AAM in the outer region, resulting in a faster size expan-

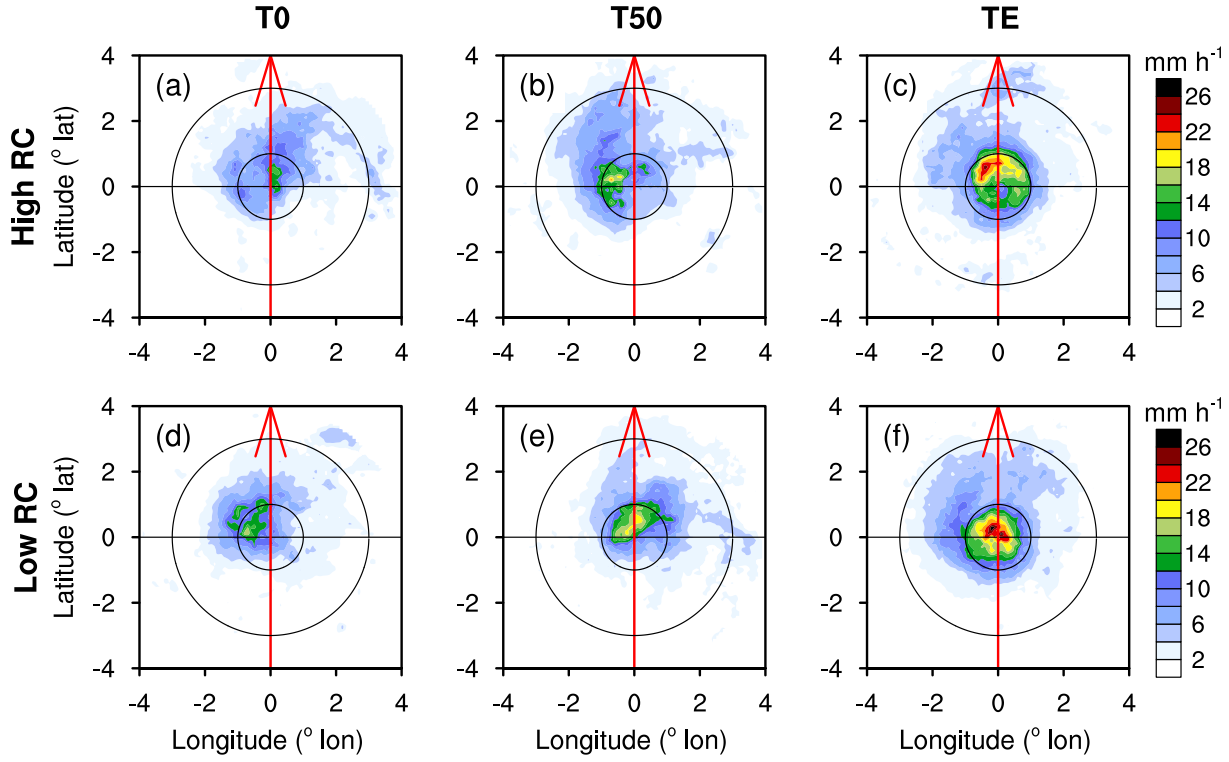

Fig. 10. Composites of the precipitation (mm h^{-1}) relative to the VWS direction at the beginning (T0), middle (T50), and the end (TE) of the development stage for (a–c) high-RC and (d–f) low-RC TCs. Two circles indicate the radii of 1° and 3° latitude from the TC center, respectively. The environmental shear direction is rotated to point northward as denoted by the vector in each figure.

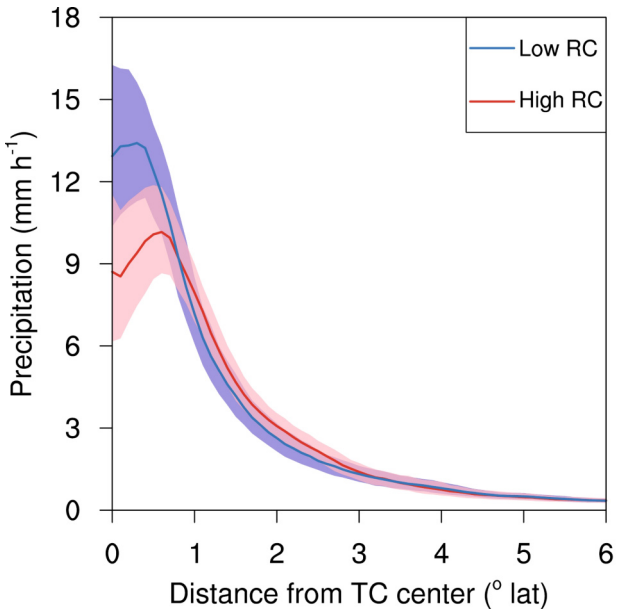

Fig. 11. Composites of the radial profile of azimuthally average precipitation rate (mm h^{-1}) during the development stage for the (red line) high-RC and (blue line) low-RC TCs within a 95% confidence interval calculated from a 1000-sample bootstrap approach (shading).

sion in the high-RC TCs.

5. Summary and Discussion

In this study, the TC size-intensity relationship over the WNP is reexamined from the perspective of individual TCs. The size and intensity of TCs from 2001 to 2020 are defined as R34 and V_{max} obtained from the JTWC best track data. Unlike the previously reported weak size-intensity correlation based on the mixture of all TC records, TC size generally exhibits a relatively strong positive correlation with intensity in individual TCs, especially during the development stage. This implies that the size-intensity correlation can be considerably affected by the calculation methods. Specifically, the intrinsic strong size-intensity correlation in individual TCs can be obscured by a large-sample framework.

Further examination points out that, although the size and intensity increase synchronously during the development stage, the size change relative to the same intensity change varies significantly among TCs, which is the root cause of the decrease in correlation when mixing up all TC samples. The size change relative to the same intensity change in individual TCs is quantified by the linear regression coefficient of R34 against V_{max} (RC), and the selected TCs are classified into high-RC and low-RC groups according to the 50th percentile of the RC. The comparison shows that, while the intensification rates in the two groups are comparable, the high-RC TCs have a greater size expansion rate than the low-RC TCs during the development stage.

Two major mechanisms are responsible for the higher expansion rate in high-RC TCs. The first is the higher latitude where the high-RC TCs occur, which favors the import of planetary angular momentum, which acts to enhance the low-level cyclonic acceleration at larger radii. The second is stronger environmental shear, promoting outer precipitation and positive feedback between diabatic heating and low-level inflow in the outer region. All of these facilitate the radially inward import of AAM, resulting in a higher expansion rate in size of the high-RC TCs.

As discussed above, in previous studies, the TC size-intensity relationship was examined based on the mixture of all TC samples (Merrill, 1984; Chavas and Emanuel, 2010; Guo and Tan, 2017). Specifically, V_{max} and R34, representing intensity and size, respectively, are two metrics that intrinsically describe the integral parts of the TC wind field structure of individual TCs; thus, the previous large-sample analysis might restrict in-depth insight into the basic physical process of TC structural evolution. The RC metric, depicting the size change relative to the same intensity change, might offer some implications for understanding the evolution of TC structure and relevant influential factors.

It should be noted that strict data screening was conducted to ensure the reliability of the statistical analysis, which certainly reduces the sample size due to the large temporal interval in the datasets. This might cause insignificant differences in the intensification rate. In addition, the exclusive role of a single factor may hardly stand out due to the synergistic effect of multiple environmental factors using the reanalysis dataset. For example, although SST and RH were regarded as key factors influencing TC size and intensity in previous studies (Hill and Lackmann, 2009; Xu and Wang, 2010b), their discrepancies between high-RC and low-RC TCs are found to be insignificant. Our ongoing work is being carried out to conduct idealized numerical simulations designed to isolate the exclusive effects of individual factors and examine their relative contributions to the TC size-intensity relationship.

Acknowledgements. This study is supported by the National Natural Science Foundation of China (Grant Nos. 41975071, 42175073) and the open project of the Shanghai Typhoon Institute, China Meteorological Administration (TFJJ202003).

Electronic supplementary material: Supplementary material is available in the online version of this article at https://doi.org/10.1007/s00376-022-1450-6.

REFERENCES

Bender, M. A., T. P. Marchok, C. R. Sampson, J. A. Knaff, and M. J. Morin, 2017: Impact of storm size on prediction of storm track and intensity using the 2016 operational GFDL hurricane model. *Wea. Forecasting*, **32**(4), 1491–1508, https://doi.org/10.1175/WAF-D-16-0220.1.

Carrasco, C. A., C. W. Landsea, and Y. L. Lin, 2014: The influence of tropical cyclone size on its intensification. *Wea. Forecasting*, **29**(3), 582–590, https://doi.org/10.1175/Waf-D-13-00092.1.

Chan, K. T. F., and J. C. L. Chan, 2012: Size and strength of tropical

cyclones as inferred from QuikSCAT data. *Mon. Wea. Rev.*, **140**(3), 811–824, https://doi.org/10.1175/Mwr-D-10-05062.1.

Chan, K. T. F., and J. C. L. Chan, 2013: Angular momentum transports and synoptic flow patterns associated with tropical cyclone size change. *Mon. Wea. Rev.*, **141**(11), 3985–4007, https://doi.org/10.1175/Mwr-D-12-00204.1.

Chan, K. T. F., and J. C. L. Chan, 2014: Impacts of initial vortex size and planetary vorticity on tropical cyclone size. *Quart. J. Roy. Meteor. Soc.*, **140**(684), 2235–2248, https://doi.org/10.1002/qj.2292.

Chan, K. T. F., and J. C. L. Chan, 2018: The outer-core wind structure of tropical cyclones. *J. Meteor. Soc. Japan*, **96**(4), 297–315, https://doi.org/10.2151/jmsj.2018-042.

Chavas, D. R., and K. A. Emanuel, 2010: A QuikSCAT climatology of tropical cyclone size. *Geophys. Res. Lett.*, **37**(18), L18816, https://doi.org/10.1029/2010GL044558.

Chavas, D. R., N. Lin, W. B. Dong, and Y. L. Lin, 2016: Observed tropical cyclone size revisited. *J. Climate*, **29**(8), 2923–2939, https://doi.org/10.1175/JCLI-D-15-0731.1.

Chen, G. H., C. C. Wu, and Y. H. Huang, 2018: The role of near-core convective and stratiform heating/cooling in tropical cyclone structure and intensity. *J. Atmos. Sci.*, **75**(1), 297–326, https://doi.org/10.1175/JAS-D-1117-0122.1171.

Cocks, S. B., and W. M. Gray, 2002: Variability of the outer wind profiles of Western North Pacific Typhoons: Classifications and techniques for analysis and forecasting. *Mon. Wea. Rev.*, **130**(8), 1989–2005, https://doi.org/10.1175/1520-0493(2002)130<1989:VOTOWP>2.0.CO;2.

DeMaria, M., and J. D. Pickle, 1988: A simplified system of equations for simulation of tropical cyclones. *J. Atmos. Sci.*, **45**(10), 1542–1554, https://doi.org/10.1175/1520-0469(1988)045<1542:ASSOEF>2.0.CO;2.

DeMaria, M., and J. Kaplan, 1999: An updated Statistical Hurricane Intensity Prediction Scheme (SHIPS) for the Atlantic and Eastern North Pacific Basins. *Wea. Forecasting*, **14**(3), 326–337, https://doi.org/10.1175/1520-0434(1999)014<0326:AUSHIP>2.0.CO;2.

Elsberry, R. L., and R. A. Jeffries, 1996: Vertical wind shear influences on tropical cyclone formation and intensification during TCM-92 and TCM-93,. *Mon. Wea. Rev.*, **124**(7), 1374–1387, https://doi.org/10.1175/1520-0493(1996)124<1374:VWSIOT>2.0.CO;2.

Guo, X., and Z. M. Tan, 2017: Tropical cyclone fullness: A new concept for interpreting storm intensity. *Geophys. Res. Lett.*, **44**(9), 4324–4331, https://doi.org/10.1002/2017gl073680.

Hersbach, H., and Coauthors, 2020: The ERA5 global reanalysis. *Quart. J. Roy. Meteor. Soc.*, **146**(730), 1999–2049, https://doi.org/10.1002/qj.3803.

Hill, K. A., and G. M. Lackmann, 2009: Influence of environmental humidity on tropical cyclone size. *Mon. Wea. Rev.*, **137**(10), 3294–3315, https://doi.org/10.1175/2009mwr2679.1.

Holland, G. J., 1983: Angular momentum transports in tropical cyclones. *Quart. J. Roy. Meteor. Soc.*, **109**(459), 187–209, https://doi.org/10.1002/qj.49710945909.

Irish, J. L., D. T. Resio, and J. J. Ratcliff, 2008: The influence of storm size on hurricane surge. *J. Phys. Oceanogr.*, **38**(9), 2003–2013, https://doi.org/10.1175/2008JPO3727.1.

Kim, D., C. H. Ho, D. S. R. Park, J. C. L. Chan, and Y. Jung, 2018: The relationship between tropical cyclone rainfall area and environmental conditions over the subtropical oceans. *J. Climate*, **31**(12), 4605–4616, https://doi.org/10.1175/JCLI-D-17-0712.1.

Kim, D., C. H. Ho, D. S. Park, and J. Kim, 2019: Influence of vertical wind shear on wind- and rainfall areas of tropical cyclones making landfall over South Korea. *PLoS One*, **14**, e0209885, https://doi.org/10.1371/journal.pone.0209885.

Kimball, S. K., and J. L. Evans, 2002: Idealized numerical simulations of hurricane–trough interaction. *Mon. Wea. Rev.*, **130**(9), 2210–2227, https://doi.org/10.1175/1520-0493(2002)130<2210:INSOHT>2.0.CO;2.

Knaff, J. A., C. Guard, J. Kossin, T. Marchok, C. Sampson, T. Smith, and N. Surgi, 2006: Operational Guidance and Skill in Forecasting Structure Change. *Proc. WMO Int. Workshop on Tropical Cyclones-VI*, San Juan, Costa Rica, WMO, 160–184. [Available on line at http://severe.worldweather.org/iwtc/document/Topic_1_5_John_Knaff.pdf]

Knaff, J. A., C. R. Sampson, M. DeMaria, T. P. Marchok, J. M. Gross, and C. J. McAdie, 2007: Statistical tropical cyclone wind radii prediction using climatology and persistence. *Wea. Forecasting*, **22**(4), 781–791, https://doi.org/10.1175/WAF1026.1.

Knaff, J. A., S. A. Seseske, M. Demaria, and J. L. Demuth, 2004: On the influences of vertical wind shear on symmetric tropical cyclone structure derived from AMSU. *Mon. Wea. Rev.*, **132**, 2503–2510, https://doi.org/10.1175/1520-0493(2004)132<2503:OTIOVW>2.0.CO;2.

Knaff, J. A., S. P. Longmore, and D. A. Molenar, 2014: An objective satellite-based tropical cyclone size climatology. *J. Climate*, **27**(1), 455–476, https://doi.org/10.1175/JCLI-D-13-00096.1.

Kurihara, Y., M. A. Bender, and R. J. Ross, 1993: An initialization scheme of hurricane models by vortex specification. *Mon. Wea. Rev.*, **121**(7), 2030–2045, https://doi.org/10.1175/1520-0493(1993)121<2030:aisohm>2.0.co;2.

Lee, C. S., K. K. W. Cheung, W. T. Fang, and R. L. Elsberry, 2010: Initial maintenance of tropical cyclone size in the Western North Pacific. *Mon. Wea. Rev.*, **138**(8), 3207–3223, https://doi.org/10.1175/2010mwr3023.1.

Li, Q. Q., Y. Q. Wang, and Y. H. Duan, 2017: A numerical study of outer rainband formation in a sheared tropical cyclone. *J. Atmos. Sci.*, **74**(1), 203–227, https://doi.org/10.1175/JAS-D-16-0123.1.

Li, T., X. Y. Ge, M. Peng, and W. Wang, 2012: Dependence of tropical cyclone intensification on the coriolis parameter. *Tropical Cyclone Research and Review*, **1**, 242–253, https://doi.org/10.6057/2012TCRR02.04.

Lin, Y. L., M. Zhao, and M. H. Zhang, 2015: Tropical cyclone rainfall area controlled by relative sea surface temperature. *Nature Communications*, **6**, 6591, https://doi.org/10.1038/ncomms7591.

Martinez, J., C. C. Nam, and M. M. Bell, 2020: On the contributions of incipient vortex circulation and environmental moisture to tropical cyclone expansion. *J. Geophys. Res.: Atmos.*, **125**(21), e2020JD033324, https://doi.org/10.1029/2020JD033324.

Matyas, C. J., 2010: Associations between the size of hurricane rain fields at landfall and their surrounding environments. *Meteorol. Atmos. Phys.*, **106**(3-4), 135–148, https://doi.org/10.1007/s00703-009-0056-1.

Merrill, R. T., 1984: A comparison of large and small tropical cyclones. *Mon. Wea. Rev.*, **112**(7), 1408–1418, https://doi.org/10.1175/1520-0493(1984)112<1408:ACOLAS>2.0.CO;2.

Musgrave, K. D., R. K. Taft, J. L. Vigh, B. D. McNoldy, and W. H. Schubert, 2012: Time evolution of the intensity and size of tropical cyclones. *Journal of Advances in Modeling Earth Systems*, **4**(3), M08001, https://doi.org/10.1029/2011ms000104.

Powell, M. D., 1990: Boundary layer structure and dynamics in outer hurricane rainbands. Part II: Downdraft modification and mixed layer recovery. *Mon. Wea. Rev.*, **118**(4), 918–938, https://doi.org/10.1175/1520-0493(1990)118<0918:BLSADI>2.0.CO;2.

Powell, M. D., and T. A. Reinhold, 2007: Tropical cyclone destructive potential by integrated kinetic energy. *Bull. Amer. Meteor. Soc.*, **88**(4), 513–526, https://doi.org/10.1175/BAMS-88-4-513.

Rogers, R., P. Reasor, and S. Lorsolo, 2013: Airborne doppler observations of the inner-core structural differences between intensifying and steady-state tropical cyclones. *Mon. Wea. Rev.*, **141**, 2970–2991, https://doi.org/10.1175/MWR-D-12-00357.1.

Smith, R. K., M. T. Montgomery, and N. van Sang, 2009: Tropical cyclone spin ‐ up revisited. *Quart. J. Roy. Meteor. Soc.*, **135**, 1321–1335, https://doi.org/10.1002/qj.428.

Smith, R. K., C. W. Schmidt, and M. T. Montgomery, 2011: An investigation of rotational influences on tropical-cyclone size and intensity. *Quart. J. Roy. Meteor. Soc.*, **137**(660), 1841–1855, https://doi.org/10.1002/qj.862.

Smith, R. K., G. Kilroy, and M. T. Montgomery, 2015: Why do model tropical cyclones intensify more rapidly at low latitudes? *J. Atmos. Sci.*, **72**, 1783–1804, https://doi.org/10.1175/JAS-D-14-0044.1.

Song, J. J., and P. J. Klotzbach, 2016: Wind structure discrepancies between two best-track data sets for Western North Pacific tropical cyclones. *Mon. Wea. Rev.*, **144**(12), 4533–4551, https://doi.org/10.1175/MWR-D-16-0163.1.

Song, J. J., Y. H. Duan, and P. J. Klotzbach, 2020: Revisiting the relationship between tropical cyclone size and intensity over the Western North Pacific. *Geophys. Res. Lett.*, **47**(13), e2020GL088217, https://doi.org/10.1029/2020gl088217.

Sun, Y., Z. Zhong, L. Yi, Y. Ha, and Y. M. Sun, 2014: The opposite effects of inner and outer sea surface temperature on tropical cyclone intensity. *J. Geophys. Res.: Atmos.*, **119**(5), 2193–2208, https://doi.org/10.1002/2013JD021354.

Tang, B, and K. Emanuel, 2010: Midlevel Ventilation's constraint on tropical cyclone intensity. *J. Atmos. Sci.*, **67**(6), 1817–1830, https://doi.org/10.1175/2010JAS3318.1.

Tao, D. D., and F. Q. Zhang, 2019: Evolution of dynamic and thermodynamic structures before and during rapid intensification of tropical cyclones: Sensitivity to vertical wind shear. *Mon. Wea. Rev.*, **147**(4), 1171–1191, https://doi.org/10.1175/mwr-d-18-0173.1.

Tsuji, H., H. Itoh, and K. Nakajima, 2016: Mechanism governing the size change of tropical cyclone-like vortices. *J. Meteor. Soc. Japan*, **94**(3), 219–236, https://doi.org/10.2151/jmsj.2016-012.

Wang, S., and R. Toumi, 2018: A historical analysis of the mature stage of tropical cyclones. *International Journal of Climatology*, **38**(5), 2490–2505, https://doi.org/10.1002/joc.5374.

Wang, Y. Q., 2009: How do outer spiral rainbands affect tropical cyclone structure and intensity? *J. Atmos. Sci.*, **66**(5), 1250–1273, https://doi.org/10.1175/2008JAS2737.1.

Weatherford, C. L., and W. M. Gray, 1988: Typhoon structure as revealed by aircraft reconnaissance. Part I: Data analysis and climatology. *Mon. Wea. Rev.*, **116**(5), 1032–1043, https://doi.org/10.1175/1520-0493(1988)116<1032:TSARBA>2.0.CO;2.

Wu, L. G., W. Tian, Q. Y. Liu, J. Cao, and J. A. Knaff, 2015: Implications of the observed relationship between tropical cyclone size and intensity over the Western North Pacific. *J. Climate*, **28**(24), 9501–9506, https://doi.org/10.1175/Jcli-D-15-0628.1.

Xu, J., and Y. Q. Wang, 2010a: Sensitivity of the simulated tropical cyclone inner-core size to the initial vortex size. *Mon. Wea. Rev.*, **138**(11), 4135–4157, https://doi.org/10.1175/2010mwr3335.1.

Xu, J., and Y. Q. Wang, 2010b: Sensitivity of tropical cyclone inner-core size and intensity to the radial distribution of surface entropy flux. *J. Atmos. Sci.*, **67**(6), 1831–1852, https://doi.org/10.1175/2010jas3387.1.

Xu, J., and Y. Q. Wang, 2018a: Dependence of tropical cyclone intensification rate on sea surface temperature, storm intensity, and size in the Western North Pacific. *Wea. Forecasting*, **33**(2), 523–537, https://doi.org/10.1175/waf-d-17-0095.1.

Xu, J., and Y. Q. Wang, 2018b: Effect of the initial vortex structure on intensification of a numerically simulated tropical cyclone. *J. Meteor. Soc. Japan*, **96**, 111–126, https://doi.org/10.2151/jmsj.2018-014.